Synthesis Dynamics of Graphite Oxide

BANNOV, A.; MANAKHOV, A.; SHIBAEV, A.; UKHINA, A.; POLČÁK, J.; MAKSIMOVSKII, E.

Thermochimica Acta
Volume 663, 10 May 2018, p. 165-175
ISSN: 0040-6031

DOI: https://doi.org/10.1016/j.tca.2018.03.017

Accepted manuscript

Title: Synthesis Dynamics of Graphite Oxide

Authors: A.G. Bannov, A. Manakhov, A.A. Shibaev, A.V. Ukhina, J. Polčák, E.A. Maksimovskii

PII: S0040-6031(18)30096-0
DOI: https://doi.org/10.1016/j.tca.2018.03.017
Reference: TCA 77967

To appear in: *Thermochimica Acta*

Received date: 1-11-2017
Revised date: 20-3-2018
Accepted date: 22-3-2018

Please cite this article as: A.G.Bannov, A.Manakhov, A.A.Shibaev, A.V.Ukhina, J.Polčák, E.A.Maksimovskii, Synthesis Dynamics of Graphite Oxide, Thermochimica Acta https://doi.org/10.1016/j.tca.2018.03.017

Synthesis Dynamics of Graphite Oxide

A.G. Bannov[a*], A. Manakhov[b], A.A. Shibaev[a], A.V. Ukhina[c], J. Polčák[f], and E.A. Maksimovskii[d,e]

[a]Department of Chemistry and Chemical Technology, Novosibirsk State Technical University, 20 K. Marx Ave., Novosibirsk, 630073 Russia

[b]National University of Science and Technology "MISiS", Moscow 119049 Russia

[c]Institute of Solid State Chemistry and Mechanochemistry, Siberian Branch of Russian Academy of Science, Kutateladze 18, 630128 Novosibirsk, Russia.

[d]Institute of Inorganic Chemistry, Siberian Branch of Russian Academy of Science, 3 Acad. Lavrentiev Ave., Novosibirsk, 630090 Russia

[e]Novosibirsk State University, 2 Pirogova Str., Novosibirsk, 630090 Russia

[f]CEITEC - Central European Institute of Technology, Brno University of Technology, Purkyňova 123, Brno, 61200 Czech Republic

* Corresponding author: tel. +7-953-772-80-89, +7-383-3460801.
E-mail: bannov.alexander@gmail.com (Alexander G. Bannov)

Highlights

- The graphite oxide synthesis dynamics was investigated by sampling technique.
- The role of H_2O_2 in the increase of GO oxidation degree was found.
- The additions of ice and H_2O_2 induce the formation of surface functional groups.
- The formation of the graphite oxide phase begins after the addition of $KMnO_4$.

Abstract

Graphite oxide synthesis dynamics were investigated using a sampling technique. The synthesis of graphite oxide was carried out by a modified Hummers' method. Small samples of the solid phase (30–50 mg) were collected from the reaction mixture and analyzed by thermogravimetric analysis, differential scanning calorimetry, scanning electron microscopy, X-ray diffraction, Raman spectroscopy, energy dissipative X-ray spectroscopy, and X-ray photoelectron spectroscopy. The strongest oxidation was detected 10 min after the start of the synthesis, i.e., after the addition of $KMnO_4$, when the formation of the graphite oxide phase with intercalated guest molecules begins. The intercalation of graphite started after 30 min of synthesis when the temperature was increased to 35°C. The addition of ice into the reaction mixture leads to the increase in the COOH group concentration, whereas the concentration of C=O groups slightly changes,

and the concentration of the C–O and C=O groups remains almost constant. It was found that the degree of oxidation of graphite oxide exhibited complex change, and H_2O_2 plays a significant role not only in the removal of impurities but also in the increase in the GO oxidation degree that is reflected by a higher concentration of oxygen-containing functional groups. Differential scanning calorimetry and thermogravimetric analysis data confirmed that the additions of ice and H_2O_2 induce the stronger formation of surface functional groups instead of intercalated guest species.

Keywords: graphite oxide, synthesis, thermal analysis, Hummers' method.

1. Introduction

Graphite oxide (GO) is a layered graphite-like material contained carbon, oxygen, and hydrogen in various ratios [1,2]. GO can be related to the group of covalent intercalation compounds, which constist of enol, keto, and epoxy groups dispersed in graphite lattice [2]. GO has the lamellar structure of the graphite with a higher interlayer spacing (d_{002} ranges between 0.562 nm and 0.902 nm [1,3]) due to the presence of oxygen-containing groups.

GO can be used for the production of different graphene- and graphite-related materials, such as graphene [4], graphene oxide [5], and exfoliated graphite [6], and for the removal of organic pollutants from water solutions [7], for the adsorption of ammonia [8], in the preparation of polymer composites [9], and as anode materials of batteries [10].

GO is predominantly synthesized by three main techniques: Hummers' [11], Brodie [12] and Staudenmaier [13] methods. The latter can be considered a modification of the Brodie method. The most often used method to obtain GO is Hummers' method. The advantage of this method is flexibility and a large potential for further modification.

There are many approaches to modifying Hummers' method. In [14], the authors used a modified Hummers' method and the Marcano-Tour method for the oxidation of graphite precursors with different particle sizes (particle sizes were < 100 μm and < 400 μm). Guerrero-Contreras et al. [15] studied the influence of the reaction temperature (5–98°C), residence time (15–120 min), and the weight of reagents ($NaNO_3$, $KMnO_4$) on the oxidation degree of GO. The O:C ratio of the samples ranged from 0.191 to 0.203 showing the weak influence of the abovementioned parameters on the oxidation degree. In [16], the authors proposed the $NaNO_3$-free method based on the partial replacement of $KMnO_4$ with K_2FeO_4, and the same approach was also used by Peng et al. [17]. The $NaNO_3$-excluding approach based on an increase in the $KMnO_4$ amount and the use of H_2SO_4/H_3PO_4 9:1 mixture was investigated in [18]. The carbon to oxygen (C/O) ratio can range from 1.0 to 2.8 wt.% depending on the synthesis method [19,20]. In some cases, using the change of concentration of reagents makes it possible to increase the C/O ratio. For example, Jankovský

et al. [21] synthesized GO by the Staudenmaier method using the various nitric acid concentrations and reached the maximum C/O atomic ratio of 4.1, determined by XPS).

Although there are many articles devoted to the synthesis of GO using classical and modified Hummers' methods, there are not sufficient data concerning the method itself, its dynamics, the number of steps, main chemical processes, etc. This work is aimed at the investigation of GO formation dynamics via modified Hummers' methods. Small samples of the solid material were taken from the mixture during the reaction performed by the modified Hummers' method, and the obtained samples were analyzed by various techniques, e.g., thermogravimetric analysis (TGA), differential scanning calorimetry (DSC), scanning electron microscopy (SEM), X-ray diffraction (XRD), Raman spectroscopy, energy dissipative X-ray spectroscopy (EDX), and X-ray photoelectron spectroscopy (XPS). Thermal analysis and XRD data confirmed the formation of an intercalated phase of graphite oxide after the addition of $KMnO_4$. Raman spectroscopy showed that the disorder degree of the material appears almost the same after 60 min of synthesis. XPS showed the complex change of the O:C ratio with synthesis time.

2. Experimental

The GO synthesis dynamics were investigated through the sampling technique. GO synthesis was carried out by the modified Hummers' method according to [22] (Fig. 1). The modified Hummers method was changed a little compared to the original Hummers method. The difference is only in the addition of reaction mixture into ice and using the excess of H_2O_2 that provide the deeper hydrolysis of graphite intercalation compounds (GICs) and the higher oxygen release after the addition of hydrogen peroxide. The effect of longer exposure time was already studied by researchers, and it was not the aim of this article. For example, in [22] it was found that the exposure time has almost no effect on the oxidation degree of graphite. But these data were obtained for a high quality nipple graphite powder (below 100 μm) that is widely used in metallurgy (particularly, electrodes). At the same time, authors in [23] reported that the role of oxidation time is not the same for various types of graphite, namely, particle size, flakes or powder, milled sample or unmilled sample. Therefore the high-quality nipple graphite and the same synthesis method were used to study the graphite oxide formation more accurately.

According to Inagaki et al. [24], the chemical oxidation of graphite powder in the presence of concentrated sulfuric acid and oxidizers such as potassium permanganate and nitric acid leads to the initial formation graphite intercalation compounds, which are unstable and when the material is exposed to water, even in the form of moisture, the material converts to graphite oxide. The material obtained that was analyzed, was taken from the reaction mixture after hydrolysis reactions caused by the water washing process.

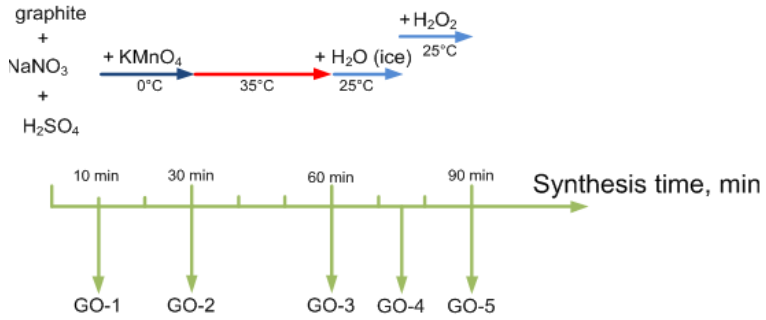

Fig. 1 – Scheme of synthesis method and the time scale of sampling

The samples were taken from a reactive mixture and investigated by the different methods described below. These samples were collected at certain time intervals during the synthesis (Table 1).

The small samples of the solid phase (30–50 mg) were collected from the reactive mixture. Briefly, high-purity (99.99%) graphite (5 g) with a particle size less than 250 μm was placed into a flask with 2.5 g of $NaNO_3$ ("chemically pure" grade; purchased by "Reactiv" ltd., Russia) and 115 mL of concentrated H_2SO_4 ("chemically pure" grade, content of sulfuric acid is 95.6%; purchased by "Reactiv" ltd., Russia). The mixture was mixed by a magnetic stirrer for 10 min and stored at a temperature of 0°C in an ice bath. The GO-1 was taken from the mixture after the start of the synthesis before the addition of $KMnO_4$. Solid, anhydrous $KMnO_4$ (chemically pure" grade; purchased by "Reactiv" ltd., Russia)was added 10 min after the start of the synthesis and was stored for 20 min at 0°C. The GO-2 sample was taken from the mixture at 30 min after the start of the synthesis. After 30 minutes, the suspension was heated to 35°C for 30 min. After heating, the GO-3 was taken from the mixture at 60 min from the start of the synthesis. Then, the mixture was poured into the flask with 230 g of ice and stored at the room temperature (25±2°C) for 15 min. A strong exothermic reaction was observed, the temperature rose temporarily to 60–65°C. The GO-4 was taken from the mixture at 75 min after the start of the synthesis. After that, the H_2O_2 ("pure for analysis" grade, weight fraction of hydrogen peroxide is 32%; "Khimprom" open joint-stock company, Russia) was added to the mixture and it was stored for 15 min at room temperature. GO-5 was taken at 90 min after the start of the synthesis, i.e., at the end of the synthesis. All samples, GO-1 – GO-5, were washed with deionized water and dried in air at 90°C over 24 h.

The GO samples were analyzed by X-ray diffraction, scanning electron microscopy, energy dissipative X-ray spectroscopy, Raman spectroscopy, thermogravimetric analysis, and differential scanning calorimetry coupled with mass spectrometry (MS). TGA and DSC measurements were performed with a synchronous thermal analyzer STA 449C Jupiter (Netzsch, Germany) under sample heating to 700°C at a heating rate of 1.0 K/min. The samples were heated in Al_2O_3 crucible in an argon atmosphere (volume flow rate 200 cm^3/min). The low heating rate was used to prevent the strong thermal expansion of the sample. TGA/DSC

measurements were carried out coupled with a quadrupole mass spectrometer QMS 403 C Aëolos (Netzsch, Germany). The surface of the samples was studied by scanning electron microscope S-3400N (Hitachi, Japan) equipped with EDX analyzer (Oxford Instruments). Raman spectroscopy was carried out using T64000 spectrometer (Horiba Jobin Yvon, Japan) (λ = 514 nm). X-ray diffraction was carried out on a DRON-3 diffractometer (Russia) using Cu Kα radiation (λ = 1.54 Å).

The chemical composition of the sample surfaces was characterized by X-ray photoelectron spectroscopy using an Axis Supra (Kratos Analytical, UK) spectrometer. The maximum lateral dimension of the analyzed area was 0.7 mm. To avoid differential charging of the samples, the spectra were acquired with charge neutralization in overcompensated mode. The spectra were subsequently normalized by shifting the sp^2 carbon component C=C to 284.4 eV. The spectra were acquired at a pass energy of 40 eV. The fitting of XPS C1s, Mn2p, S2p, and O1s was done using the CasaXPS software (version 2.3.17) after subtraction of the Shirley-type background employing Gaussian–Lorentzian (G-L) peaks with the fixed G-L percentage of 30%. The values of the binding energies of C and O environments were taken from the literature [25,26].

3. Results and Discussion

3.1 TGA and DSC

The results of thermal analysis of the samples are presented in Fig. 2.

a

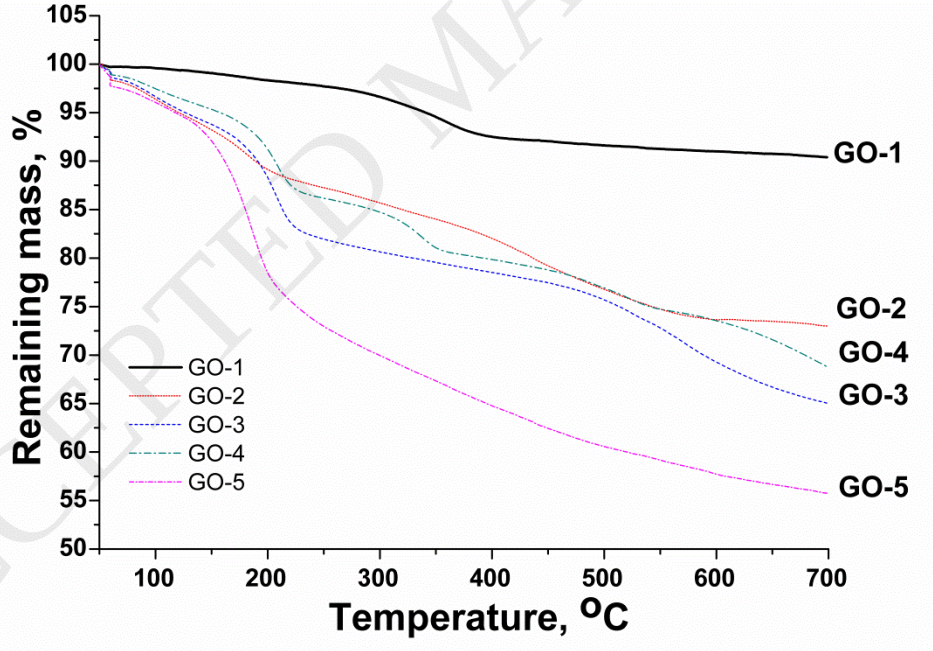

b

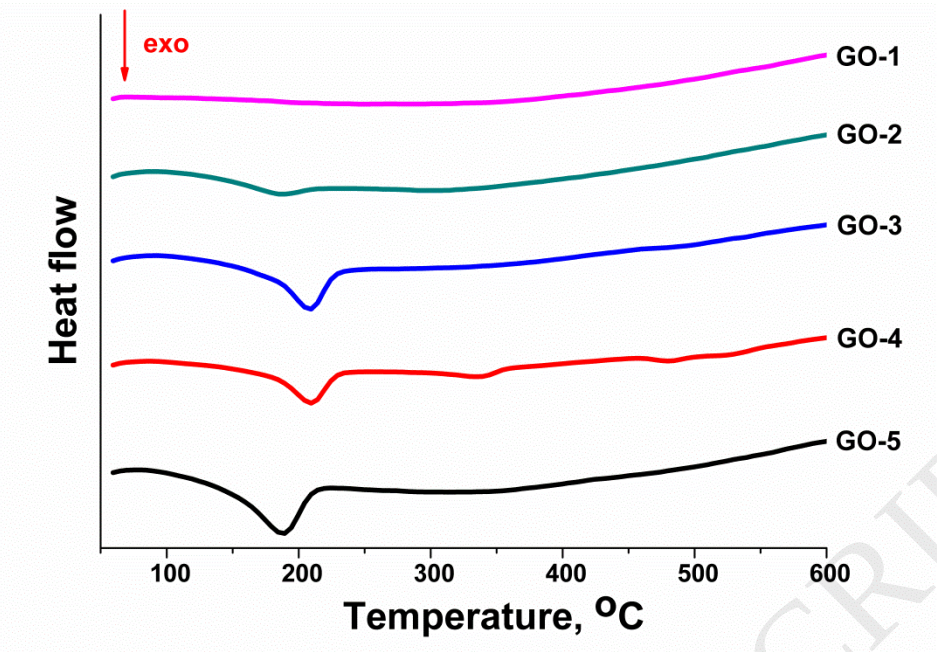

Fig. 2 – TGA (a) and DSC (b) data of the samples obtained (Ar flow rate was 200 cm^3/min; Al_2O_3 crucible; heating rate was 1.0 K/min)

Pristine graphite shows a TGA curve without a change of weight during heating up to 700°C. GO-1 shows a different behavior during heating, with a strong mass loss of approximately 9.6% (Table 2). An even greater mass loss was detected for the GO-2 sample collected from the reaction mixture after the addition of $KMnO_4$. The highest mass loss was observed for the GO-5 sample. The DSC curves shown in Fig. 2b indicate the reduction of the GO samples by the presence of an exothermic peak in a range of 160–210°C. The peak can be observed in the GO-2 sample, whereas the GO-1 had no peak, confirming that the intercalation of graphite did not start at this stage.

It is worth noting that the range in which the DSC peak of GO reduction located is lower than the reported values. For example, Talyzin et al. measured the exfoliation temperature of Hummers'-GO within a range of 213–220°C [3]. The comparison of the thermal behavior of the GO-5 sample with the literature data of the thermal exfoliation obtained by TGA/DSC is shown in Table 3. The heat release, determined as the area of DSC exothermal peak, varied in the range of 78–652 J/g. The value of enthalpy of the GO reduction process for GO-5 (652 J/g) was lower than that usually reported in the literature. For example, Juan et al. [27] reported GO exothermal heat of 490.1 J/g. A comparison of the heat release data is also summarized in Table 3.

The reduction of GO can also be confirmed by mass spectrometry data coupled with the TGA/DSC results (*Figs. S1 in Supplementary materials*) by the increase in the ion current of m/z = 44 amu (CO_2) in a

temperature range corresponding to the DSC peak of GO reduction. Even though the end of DSC peak ranges from 200 to 214°C, the CO_2 release still occurs at the temperature higher than 250-300°C, confirming the conversion of the functional groups attached to carbon skeleton under heating [33]. It was reported in [34] that lactone groups were released in a range of 250–300°C, which was also accompanied by the release of CO_2, whereas carboxyl groups was released between 100 and 250°C. Barton et al. [35] reported the release of CO_2 from the groups, containing C=O fragment (carboxylic acids and anhydrides, esters) at 250°C. According to our TGA/DSC+MS data, it is not possible to separate these two types of groups, because their peaks overlap. It must be considered that there are two overlapping peaks for the release of CO_2 (150–300°C and 300–700°C), and this can be attributed to the evolution of the gas phase from the intercalated guest molecules (first low-temperature peak), e.g. mainly represented by water molecules, and decomposition of surface functional groups.

The GO-4 sample showed a different DSC curve behavior compared to other samples (Fig. 3). There were more peaks observed in addition to the GO reduction peak: an exothermal peak at 307–360°C (maximum at 335°C) and a complex peak in a range of 459–549°C, which consisted of two peaks with a maximum at 483°C and 532°C (Fig. 3). It is worth noting that these peaks were also observed in GO-3 sample, but the level of the DSC signal was very low. The absence of these two high-temperature peaks can be linked with the addition of H_2O_2 to the reaction mixture. It can be suggested that these two peaks can be attributed to manganese-containing compounds that appear in the GO-3 and GO-4 samples, the presence of which was also demonstrated by XRD and XPS in sections 3.2 and 3.3.

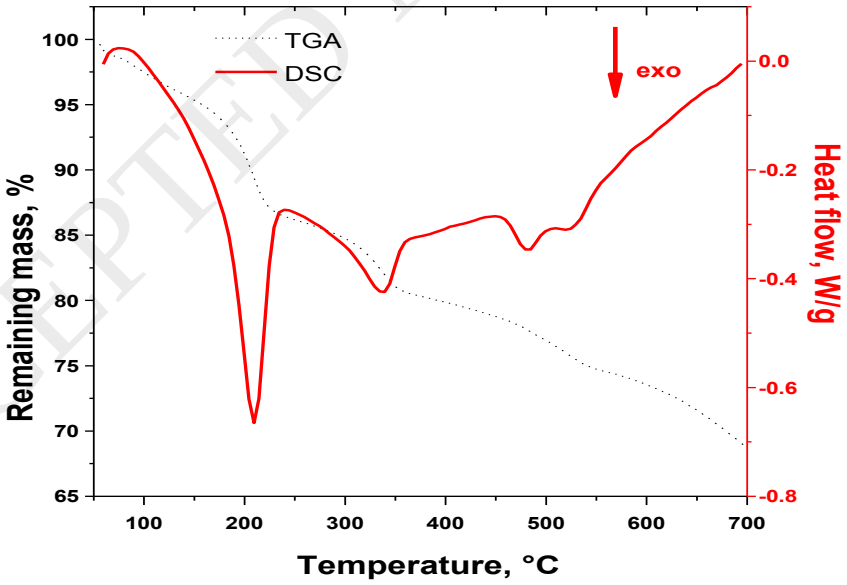

Fig. 3 – TGA and DSC curves of GO-4 sample (Ar flow rate was 200 cm^3/min; Al_2O_3 crucible; heating rate was 1.0 K/min)

The derivative of the TGA signal (DTG) is also a very informative tool to study the formation of graphite oxide, and the data are shown in Fig. 4.

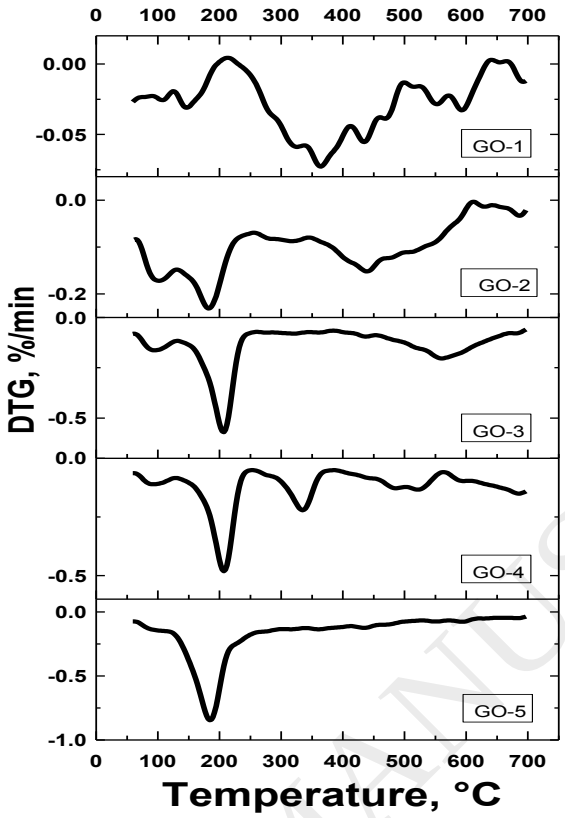

Fig. 4 – DTG curves of the GO samples (Ar flow rate was 200 cm^3/min; Al_2O_3 crucible; heating rate was 1.0 K/min)

The increase in the reaction time induced the appearance of a broad DTG peak in the range of 145–207°C. In [36], the authors attributed this peak to the evaporation of water; however, it corresponds to the reduction of GO because it matches the respective DSC peak. The GO-1 sample exhibited a lower mass loss rate. GO-2 shows the appearance of two DTG peaks: the first one with the maximum of 93°C and the second with the maximum of 180°C, indicating the presence of two processes linked with the weight loss during heating. Most likely, the first peak can be attributed to the release of water from between the graphene layers, and the second peak is attributed to the release of CO_2 because of the decomposition of functional groups. These two peaks separate, and the first peak shifts to a lower temperature as the second peak shifts to a higher temperature. GO-4 and GO-5 show only the high-temperature peak at approximately 130–210°C related to the GO reduction.

3.2 SEM, EDX, and XRD

The GO formation dynamics can also be estimated from the C:O ratio measured by EDX (Fig. 5a).

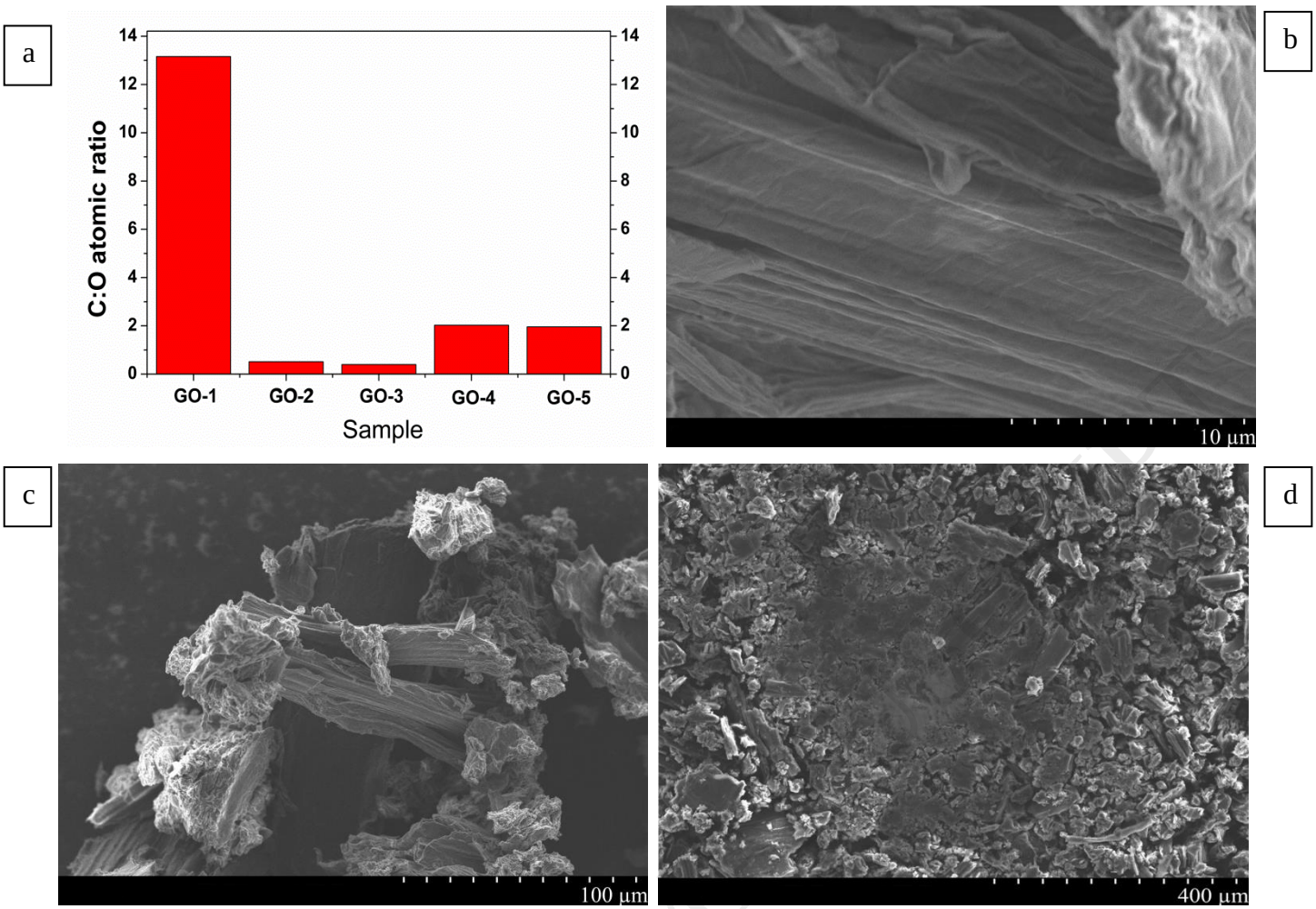

Fig. 5 – C:O atomic ratio of the GO samples obtained by EDX (a) and SEM images of GO-5 sample (b, c, d) obtained using the secondary electron detector

According to the results, the GO-2 and GO-3 samples contained more oxygen compared to the other samples. C:O ratios of 0.51 and 0.54 were found for GO-2 and GO-3, respectively. The C:O ratio of GO-4 and GO-5 equals 2.0 for both samples. The GO-4 and GO-5 samples contained 65.7 and 65.1 at.% of carbon, 32.4 and 33.1 at.% of oxygen, respectively, that was close to the EDX data reported for Tour's method and GO obtained by the rapid synthesis using H_2SO_4, H_3PO_4, and $KMnO_4$ [20]. One can note that the sulfur concentration (1.15 at.% and 1.26 at.% for the GO-4 and GO-5 samples, respectively) was almost the same as was determined for Tour's method in [20].

The SEM images of the samples are almost the same, and the micrographs are shown in Figs. 5b-5d. The SEM images of the GO-1 – GO-4 samples are presented in *Fig. S2 in Supplementary materials*. The surface texture of the GO samples was almost the same.

The phase composition transformation of graphite during its oxidation by modified Hummers method can be monitored by XRD (Fig. 6).

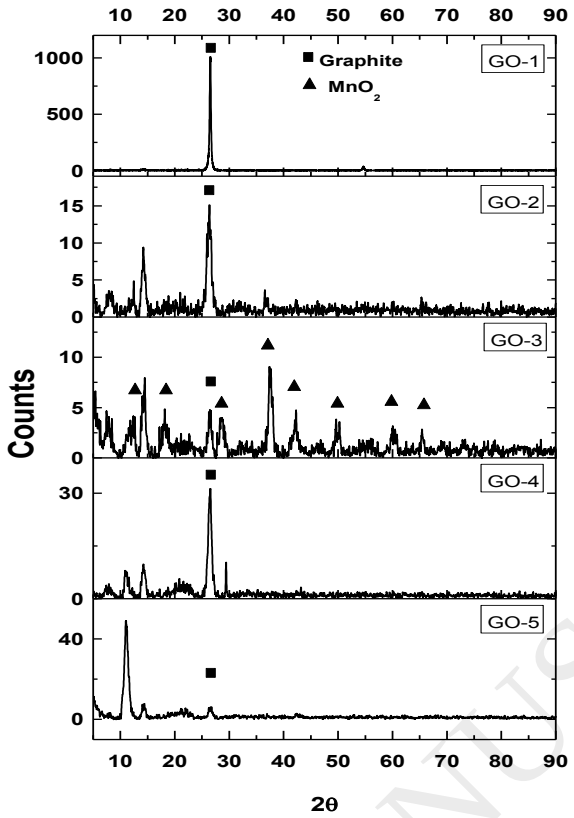

Fig. 6 – XRD patterns of the GO samples (Cu Kα radiation, λ = 1.54 Å)

The graphite phase was found in the XRD patterns (reflection at 2θ = 26°) of the entire GO series. The concentration of the graphite phase decreased increased synthesis time. As seen from Fig. 6, the GO-1 sample contained only the graphite phase, which was also confirmed from the C:O ratio determined by EDX (C:O ratio equals to 13). The peaks with a diffraction angle 2θ below 26° can be attributed to the formation of the GO phase. The wide set of XRD peaks in this region is caused by the intercalation of guest species. There is a typical graphite oxide *002* reflection available in the XRD pattern, which can be attributed to the GO formation, namely, at 2θ = 11.1° (interlayer distance equals to 7.969 Å and 7.984 Å for the GO-4 and GO-5 samples, respectively), and this value is in agreement with the data obtained for GO synthesized by Hummers method [37]. These interlayer distances depend on the hydration level [38] since water molecules are associated with functional groups between graphene layers [39]. In [33] authors suggested that interlayer spacing is mainly determined by hydroxyl groups bonded on both sides of the carbon skeleton. In addition, the weak peak at 2θ = 14.2° corresponding to GO with a different degree of intercalation has been observed. In [20] the presence of the *100* reflections (around 2θ = 42.6°) was detected for GO samples indicating the long range ordering, and they were presented in the spectra of the GO-2 – GO-5 samples.

The addition of $KMnO_4$ to the reaction mixture led to the formation of the MnO_2 phase in the GO-3 sample. Manganese oxide (MnO_2), corresponding to the PDF database *#72-1982*, appeared in the GO-3 sample. The amount of MnO_2 in GO-3 was estimated from the Powder Cell 2.4 software. The sample

consisted of 31.8 at.% of the MnO_2 phase and 67.2 at.% of the graphite phase. The GO phase formation was observed for GO-2. Additionally, the peaks attributed to GO were observed on the XRD pattern.

The disappearance of the phases corresponding to the manganese-containing compounds in the GO-4 spectrum could result from the addition of H_2O_2, which induces the transformation of these compounds to the soluble state (e.g., $MnSO_4$) and from their removal during sample washing (1). The difference between GO-4 and GO-5 is a decrease in the *002* peak intensity, which is caused by the strong oxidation of the graphite phase by oxygen formed after the addition of H_2O_2, which led to the gradual oxidation of the residual graphite phase presented in the sample.

$$MnO_2 + H_2O_2 + 2H^+ \rightarrow O_2 + Mn^{2+} + 2H_2O \quad (1)$$

3.3 Raman spectroscopy

Typical Raman spectra are shown in Fig. 7. The spectra consist of two main peaks, the D peak (1349–1356 cm^{-1}) corresponding to a disordered structure, and the G peak (1576–1590 cm^{-1}), which is attributed to the graphitic structure (Table 4). GO-3 and GO-4 spectra are presented in *Fig. S3 in Supplementary materials*.

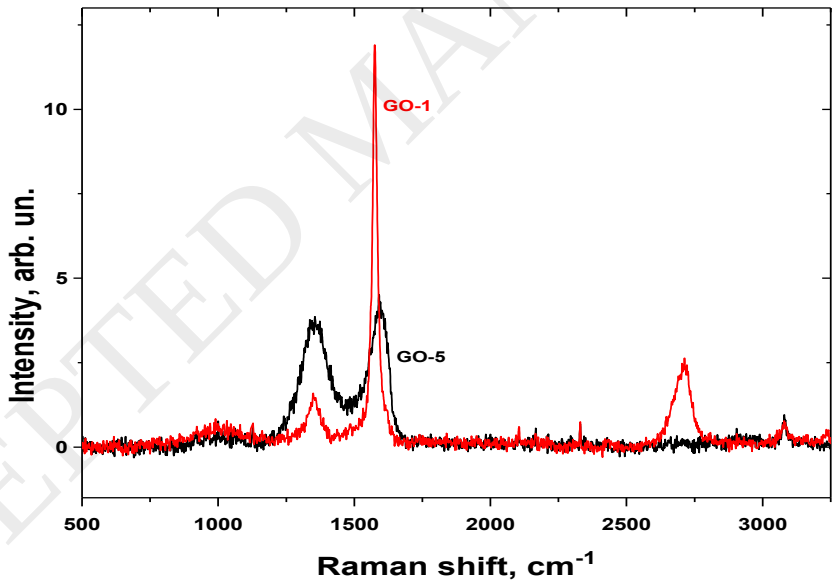

Fig. 7 – Raman spectra of the GO-1 and GO-5 samples (λ = 514 nm)

The ratio of the D and G peaks I(D)/I(G) provides information about the degree of disorder of the carbon material [40]. Thus, the GO-1 sample is closer to the graphite because it was collected only 10 min after the start of the synthesis, and the formation of graphite oxide had not yet begun. The strong luminescence makes it hard to identify the D and G peaks in the GO-2 sample, which was also reported in [21]. The GO-3 – GO-5 samples had a similar I(D)/I(G) range from 0.88 to 0.91, which decreased with

reaction time. The I(D)/I(G) ratios of the GO-4 and GO-5 samples are close to that of reported for graphite oxides synthesized using the Tour, Hofmann, and Hummers methods in [19].

The decrease of the I(D)/I(G) ratio is linked to the growth of the sp^3 carbon atoms fraction [41], and it correlates well with the sp^3 component of the C1s photoelectron spectrum described in the next section. The stronger the oxidation, the narrower G peak was, and its position shifted from 1580.8 cm^{-1} (GO-3) to 1590.5 cm^{-1} (GO-5). D peak also became narrow with the increase of reaction time.

3.4 XPS

The results of the XPS fitting of the C1s spectra are summarized in Table 5. XPS survey spectra are presented in *Fig. S4 in Supplementary materials*.

According to the literature [19,20] the most intense peak at 284.3–284.4 eV corresponds to sp^2-hybridized carbon atoms (C=C bonds in the graphite structure) (Fig. 8).

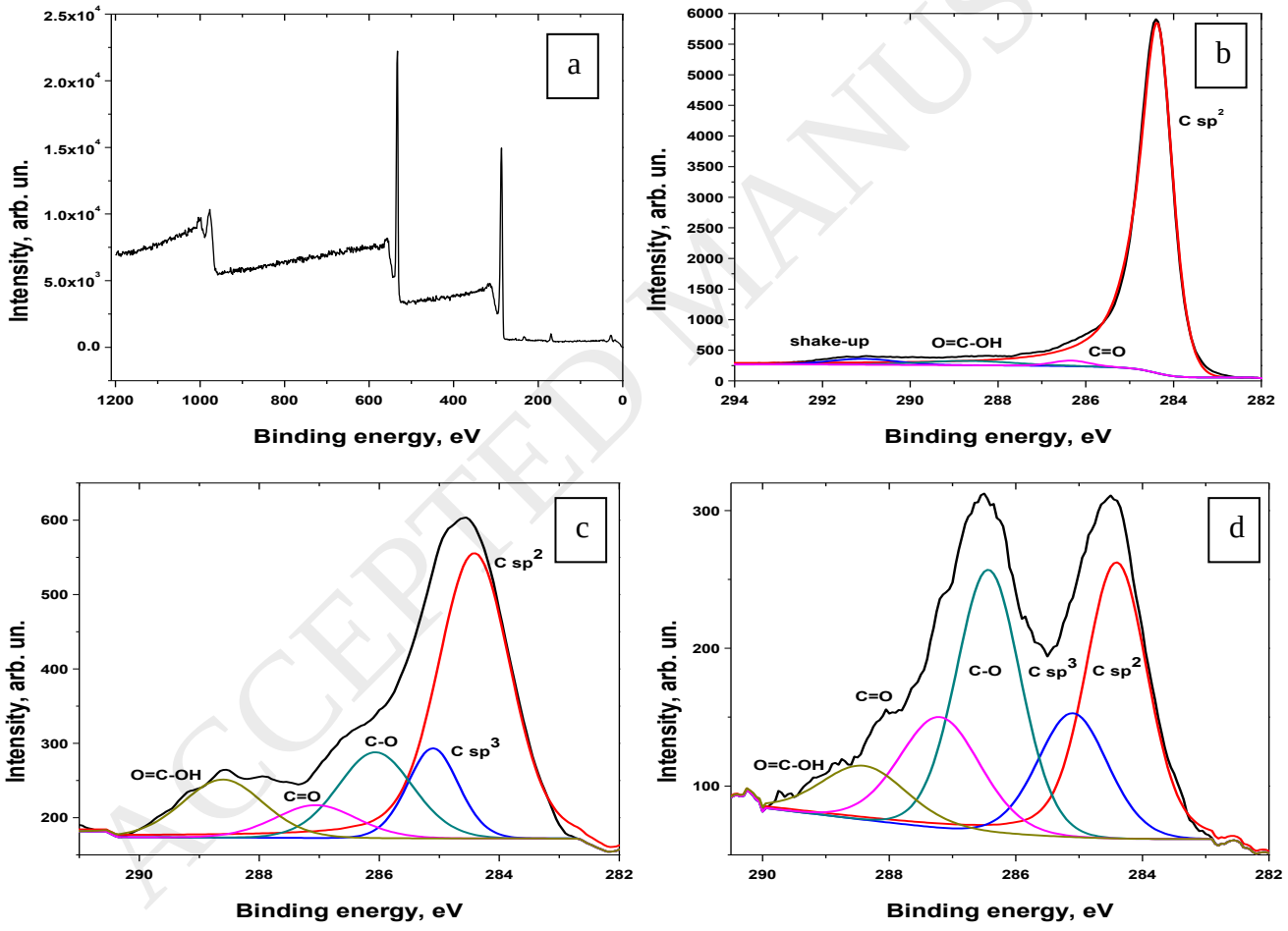

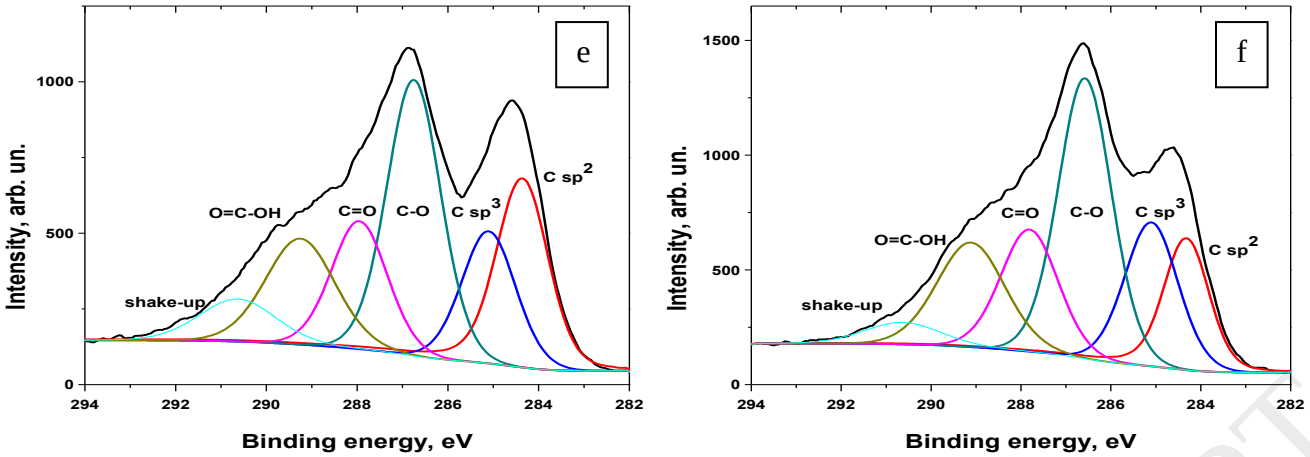

Fig. 8 – XPS spectrum of the GO-5 sample (a) and C1s XPS spectra of b – GO-1, c – GO-2, d – GO-3, e – GO-4, f – GO-5

The second peak at 285.0–285.2 eV corresponds to the carbon atoms in the sp^3 hybridization (C–C, C–H bonds). The relative intensity of these two peaks is used to determine the degree of graphitization of the carbon materials [21], and this value was as follows: GO-1 (100%), GO-2 (78.5%), GO-3 (51.0%), GO-4 (29.4%), and GO-5 (24.3%). Three other peaks are visible in the regions of 286.2–286.7, 287.1–287.9, and 288.4–289.4 eV correspond to carbon atoms chemically bonded to oxygen, e.g., carbon single-bonded to oxygen (C–O), carbon double-bonded to oxygen (C=O), and carboxyl/ester C(O)O groups, respectively [26]. There were also shake-up satellites at approximately 290.5–290.6 eV corresponding to π–π* interactions. The data on the concentration of elements in the sample are presented in Table 5. The content of carbon in the sp^2 form in GO-1 confirms that the sample had a composition similar to graphite with the formation of surface oxygen-containing groups. The addition of $KMnO_4$ induces the strong oxidation of graphite (O – 51.6±1.8 at.%), although there was no DSC peak clearly identifying the exothermic reduction of GO during heating (GO-2 sample). However, the GO-3 sample shows a higher carbon content than that of GO-2, but there is a strong DSC peak for its reduction, indicating the formation of graphite intercalation compounds [42]. The addition of ice or H_2O_2 led to an oxygen concentration of 31.9±0.4 at.% (GO-5). Usually, authors have mentioned that H_2O_2 is used only for removing impurities [16]. However, here we have shown that the addition of this compound provides more complete oxidation of GO, and it is confirmed by O:C ratio (Table 5).

The O1s XPS spectra consist of three main components: oxygen double-bonded to carbon C=O (531.5–532.0 eV), oxygen single-bonded to carbon C–O (532.4–532.9 eV), peroxide oxygen single-bonded to another oxygen O–O (535.4–532.9 eV), and O–OC groups (533.9–534.3 eV) (Fig. 9). The O1s spectrum of GO-1 is represented by two components: oxygen from sulfates SO_4^{2-} at 533.1 eV (36.2±2.7 at.%) and C=O at 531.5 eV (63.8±2.6 at.%). However, there are also other components visible in the O1s spectra of the other samples. The O1s spectrum of the GO-2 sample clearly shows the formation of MnO_2 after the

addition of $KMnO_4$ by the appearance of a component at 529.6 eV corresponded to oxygen double bonded with manganese, and its area shows that 63.56±2.8 at.% of oxygen was bonded with manganese. The GO-2 O1s spectrum also contained C–O (9.54±2.8 at.%) and C=O (26.91±4.3 at.%) components. The GO–3 O1s spectrum also contains a MnO_2 component (41.2±4.8 at.%), C–O (9.1±5.9 at.%), C=O (26.1±9.6 at.%), and a manganese oxyhydroxide component MnOOH (23.6±11.8 at.%). It can be suggested that after the addition of ice into the reaction mixture, the MnO_2 component disappeared, confirming its conversion to the water-soluble compounds of manganese (e.g., $MnSO_4$) as a result of interaction of sulfuric acid formed during hydrolysis of graphite bisulphate which is released to the solution and interacts with manganese dioxide.

The data of Mn content presented in Table 5 and in Fig. 6 are different. According to Fig. 6, MnO_2 was detected in GO-3 but there are no manganese-containing phases in XRD spectrum of GO-2. According to Table 5, GO-2 contains 18.7±0.8 at. % Mn. The fact that XRD and XPS data are not in accordance is most probably related to the difference of probing depth of these two analytical methods. XRD probes the bulk of the material, whereas XPS provides the information regarding the chemical composition of the extreme surface (top 5 nm). If the MnO_2 is available mostly on top of the surface then only XPS can determine it. The absence of manganese-containing phases is also due to the limit of the detection of phase which is 5% for XRD, and this fact indicates that the content of these phases is low enough to be detectable by the XRD.

The C–O (50.3±2.2 at.%), O–O (24.2±2.8 at.%), and O–OC (25.5±2.4 at.%) components in the GO–4 O1s spectrum indicated the strong hydrolysis of GICs with the formation of graphite oxide. The sample collected after the H_2O_2 addition (GO-5) shows the same components in the O1s spectrum, but the concentration of oxygen in the form O–OC increased (C–O (50.82±3.0 at.%), O–O (19.43±2.7 at.%), and O–OC (29.74±2.7 at.%)). This increase can be linked with the oxygen transformation from the O–O form to the O–OC group.

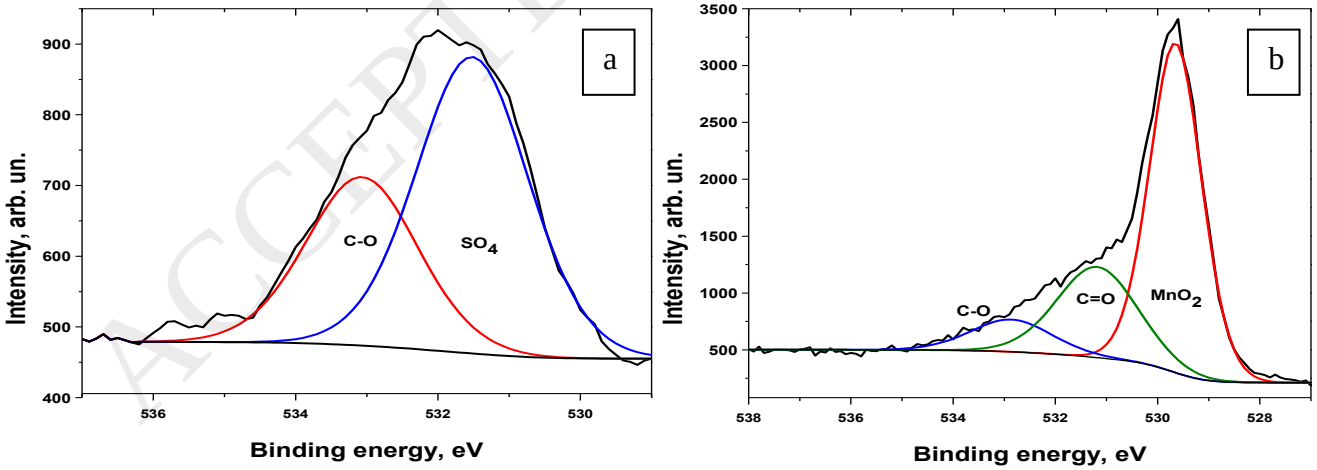

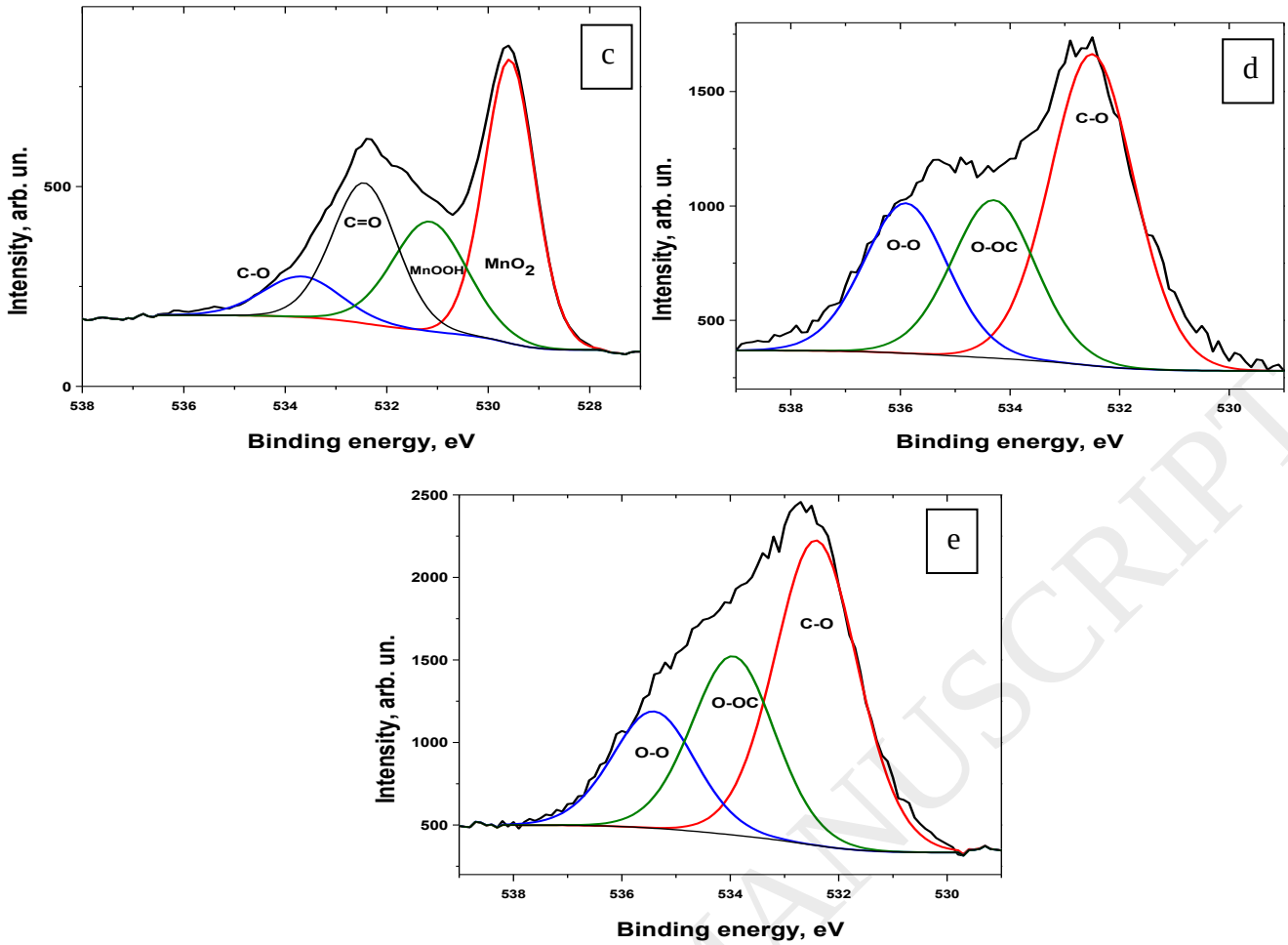

Fig. 9 – O1s XPS spectra of the samples: a – GO-1, b – GO-2, c – GO-3, d – GO-4, e – GO-5

From the Mn2p XPS spectrum it can be found that the Mn2p signal was detected only in the GO-2 and GO-3 samples, confirming the presence of manganese in two forms: MnO_2 (six peaks $Mn(2p_{3/2})$ in a range of 646.7–641.8 eV) and Mn^{3+} (640.9 eV) (Figs. 10a and 10b) [43].

The presence of sulfuric acid in the reaction mixture predetermines the presence of sulfur in GO originating from sulfate anions [3]. The S2p spectrum shows the presence of two components corresponding to $S(2p_{1/2})$ and $S(2p_{3/2})$, and the spectrum can be clearly seen only for GO-1 (Fig. 10c), confirming the formation of graphite bisulfate [44,45] in a reaction medium. The presence of graphite bisulphate was also reported in [46].

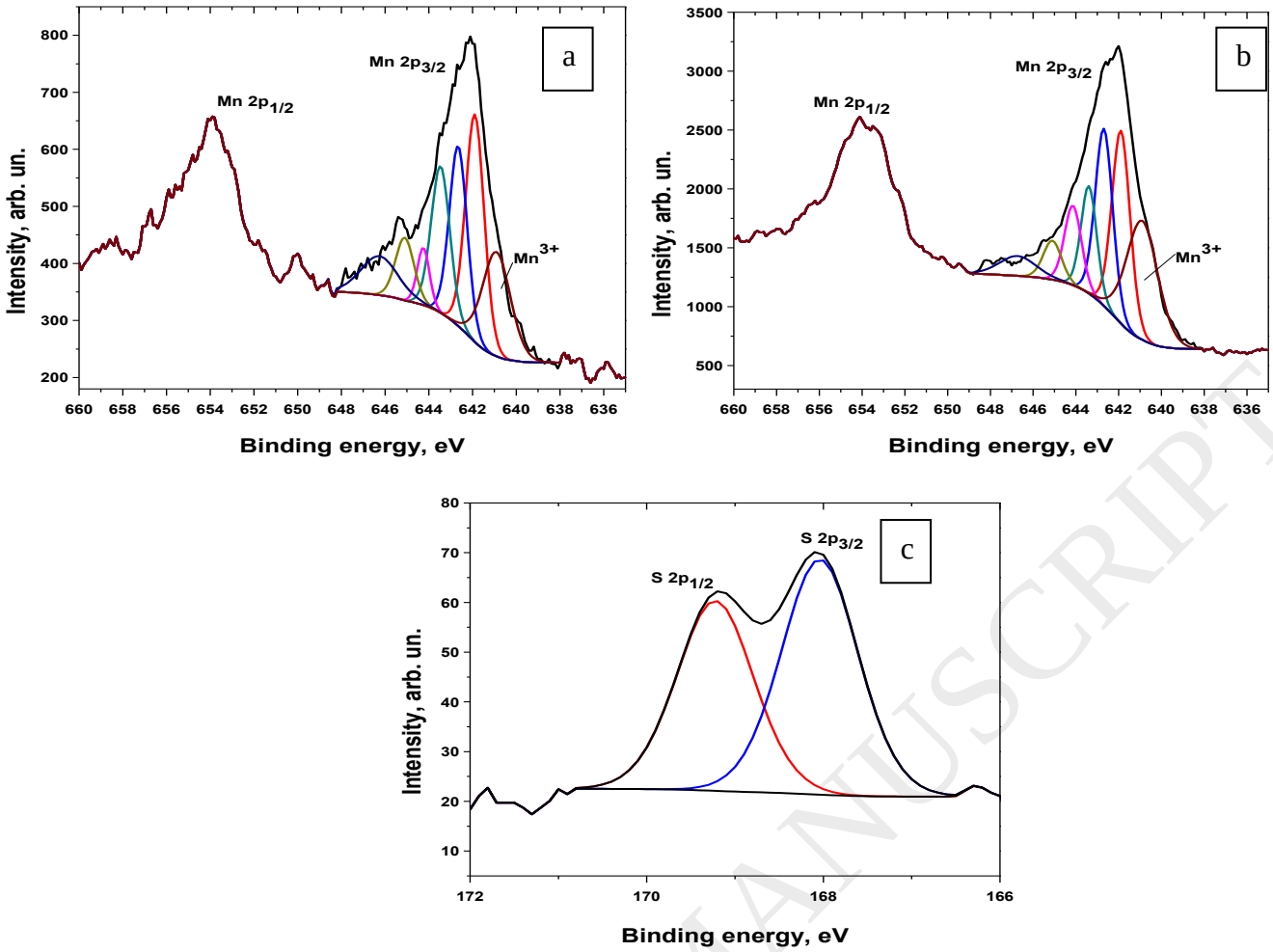

Fig. 10 – Mn2p spectra of GO-2(a) and GO-3(b); S2p spectra of GO-1 (c)

3.5 GO formation mechanism

Some authors reported that manganese-containing compounds, such as Mn_2O_7 and MnO_3^+, induce the oxidation of graphite [46–48]. However, they did not mention the role of $NaNO_3$, which is also present in the reaction mixture and provides the formation of graphite bisulphate [1,44]. Sulfuric acid itself cannot form bisulfate upon the interaction with graphite, and therefore, nitric acid plays the role of oxidizer [45]. Addition of $NaNO_3$ provides the presence of NO_3^- ions in a strong acidic medium assisting the formation of graphite bisulfate. The GICs formed transform to graphite oxide even at the addition of small amounts of water. In this way, the formation of graphite bisulfate occurs until $KMnO_4$ is added. The addition of $KMnO_4$ to the reaction mixture and the process over 20 min at 0°C do not lead to the strong oxidation of graphite, but the temperature increase to 35°C induces the appearance of a strong exothermic DSC peak and a sharp decrease in the *002* peak intensity in the XRD patterns. Of course, MnO_4^- has a high oxidation potential, which, in combination with a strong acidic mixture (H_2SO_4–HNO_3), leads to the stronger formation of GICs; the complex role of the acidic mixture (H_2SO_4–HNO_3) and the MnO_4^- are likely responsible.

The addition of ice into reaction mixture induces the hydrolysis of GICs with the formation of a higher content of functional groups. However, the increase in the concentration of carboxyl groups is predominantly (according to XPS) induced by the addition of ice, while the concentration of the C–O and C=O groups remains almost constant. Notably, the role of H_2O_2 in the oxidation of graphite is also important. The increase in the total mass loss of the samples is determined by TGA and is 31.25% and 44.0% for the GO-4 and GO-5 samples, respectively, indicating the stronger oxidation of graphite due to higher oxygen release after the addition of H_2O_2. According to TGA data, the weight loss of samples GO-1 – GO-3 mainly occurs at temperatures corresponding to GO reduction (up to 210–220°C) and decomposition of functional groups (above 300-400°C). Meanwhile, the GO-4 and GO-5 samples have the weight loss in a temperature range between GO reduction peak onset and peak end (determined by DSC), which is 8.2% (GO-4) and 12.5% (GO-5) within 184–228°C and 160–202°C, respectively, and further temperature increase makes the weight loss difference higher. This fact confirms that the additions of ice and H_2O_2 induce the larger formation of surface functional groups instead of intercalated guest molecules, such as sulfate ions, water etc. These oxygen-containing functional groups are introduced into graphene layers during formation of graphite oxide [47].

There are two processes that occur during GO synthesis: the formation of surface oxygen-containing groups and the formation of intercalated guest molecules. The first process occurs before the addition of ice addition into the reaction mixture, and the functional groups (C=O, C–O, C(O)O) mainly form on the surface of the material as a result of oxidation of the graphite sheets. The second process leads to the formation of intercalated guest species accompanied by a decrease in the sp^2 carbon concentration in GO, and it occurs before the addition of ice.

According to the TGA and XPS data, the limiting stage of graphite transformation to GO can be found from a time range of 30–60 min, when the temperature increased to 35°C. The intensifying effects, such as ultrasonication, intensive mixing, circulation mixing, can be used to accelerate the process at this stage.

In conclusion, it is worth noting that there is a possibility to synthesize the different types of graphite oxide, which can be used for obtaining the graphene oxide, graphene, and exfoliated graphite, using a modified Hummers' technique controlled only by the reaction time. Moreover, the synthesis of graphite oxide by the modified Hummers' method can be divided into separate parts from which at least three different types of GO exhibiting different oxidation degrees can be obtained. These graphite oxides exhibit different texture characteristics and chemical compositions after their exfoliation.

Conclusions

Different stages of GO formation using the modified Hummers' method were studied using a sampling technique that included the analysis of small samples of material removed from the reaction mixture during synthesis. The possibility to obtain the different types of graphite oxides by this method was shown.

TGA/DSC and XRD data confirmed the formation of the intercalated phase of graphite oxide at 60 min from the start of the synthesis (20 min after the addition $KMnO_4$). Raman spectroscopy shows that the degree of disorder of the material appears at almost the same value after 60 min of reaction. XPS shows the complex change of the O:C ratio during the synthesis. It confirms that the addition of H_2O_2 plays a significant role, not only in the removal of impurities but also in the increase in the GO oxidation degree that is reflected by the higher concentration of C–O, C=O, and COOH groups. The addition of ice into the reaction mixture leads to an increase in the concentration of the COOH group, whereas the concentration of C=O groups only changes slightly.

Acknowledgments

The research was carried out with the support of Stipend of the President of Russian Federation for Young Researchers SP-547.2018.1. A. Manakhov acknowledges the financial support of the Ministry of Education and Science of the Russian Federation in the framework of Increase Competitiveness Program of NUST “MISiS” (№ K4-2016-005), implemented by a governmental decree dated 16th of March 2013, N 211. Part of the work was carried out with the support of CEITEC Nano Research Infrastructure (MEYS CR, 2016–2019) and CEITEC 2020 (LQ1601) with financial support from the Ministry of Education, Youth and Sports of the Czech Republic (MEYS CR) under the National Sustainability Programme II.

References

[1] T. Nakajima, A. Mabuchi, R. Hagiwara, A new structure model of graphite oxide, Carbon N. Y. 26 (1988) 357–361. doi:10.1016/0008-6223(88)90227-8.

[2] D.D.L. Chung, Review Graphite, J. Mater. Sci. 37 (2002) 1475–1489.

[3] A. V. Talyzin, G. Mercier, A. Klechikov, M. Hedenström, D. Johnels, D. Wei, D. Cotton, A. Opitz, E. Moons, Brodie vs Hummers graphite oxides for preparation of multi-layered materials, Carbon N. Y. 115 (2017) 430–440. doi:10.1016/j.carbon.2016.12.097.

[4] M. Kang, D.H. Lee, J. Yang, Y. Kang, H. Jung, RSC Advances Simultaneous reduction and nitrogen doping of graphite oxide by using electron beam irradiation, RSC Adv. 5 (2015) 104502–104508. doi:10.1039/C5RA20199C.

[5] T. Soltani, B. Kyu Lee, A benign ultrasonic route to reduced graphene oxide from pristine graphite, J. Colloid Interface Sci. 486 (2017) 337–343. doi:10.1016/j.jcis.2016.09.075.

[6] A. Mackova, M. Mikulics, M. Pumera, Insight into the Mechanism of the Thermal Reduction of Graphite Oxide : Deuterium-Labeled Graphite Oxide Is the Key, (2015) 5478–5485.

[7] S. Wu, L. Yu, F. Xiao, X. You, C. Yang, J. Cheng, Synthesis of aluminum-based MOF/graphite oxide composite and enhanced removal of methyl orange, J. Alloys Compd. 724 (2017) 625–632. doi:10.1016/j.jallcom.2017.07.095.

[8] M. Seredych, T.J. Bandosz, Combined role of water and surface chemistry in reactive adsorption of ammonia on graphite oxides, Langmuir. 26 (2010) 5491–5498. doi:10.1021/la9037217.

[9] J. Bian, H.L. Lin, F.X. He, L. Wang, X.W. Wei, I.-T. Chang, Y. Lu, Comparative study on the natural rubber nanocomposites reinforced with carbon black nanoparticles and graphite oxide nanosheets, Polym. Compos. 38 (2015) 1427–1437. doi:10.1002/pc.

[10] Y. Sun, J. Tang, K. Zhang, J. Yuan, J. Li, D.-M. Zhu, K. Ozawa, L.-C. Qin, Comparison of reduction products from graphite oxide and graphene oxide for anode applications in lithium-ion batteries and sodium-ion batteries, Nanoscale. 9 (2017) 2585–2595. doi:10.1039/C6NR07650E.

[11] J. William S. Hummers, R.E. Offeman, Preparation of Graphitic Oxide, J. Am. Chem. Soc. 80 (1958) 1339. doi:10.1021/ja01539a017.

[12] B.C. Brodie, On the Atomic Weight of Graphite, Philos. Trans. R. Soc. London. 149 (1859) 249–259. doi:10.1098/rstl.1859.0013.

[13] D. Salze, D. Doppel-, D. Reaction, L. Staudenmaier, D. Substanz, I. Zeit, Verfahren zur Darstellung der Graphitsaure, Ber. Dtsch. Chem. Ges. 31 (1898) 1481–1487. doi:10.1002/cber.18980310237.

[14] E.M. Deemer, P.K. Paul, F.S. Manciu, C.E. Botez, D.R. Hodges, Z. Landis, T. Akter, E. Castro, R.R. Chianelli, Consequence of oxidation method on graphene oxide produced with different

size graphite precursors, Mater. Sci. Eng. B Solid-State Mater. Adv. Technol. 224 (2017) 150–157. doi:10.1016/j.mseb.2017.07.018.

[15] J. Guerrero-Contreras, F. Caballero-Briones, Graphene oxide powders with different oxidation degree, prepared by synthesis variations of the Hummers method, Mater. Chem. Phys. 153 (2015) 209–220. doi:10.1016/j.matchemphys.2015.01.005.

[16] H. Yu, B. Zhang, C. Bulin, R. Li, R. Xing, High-efficient Synthesis of Graphene Oxide Based on Improved Hummers Method, Sci. Rep. 6 (2016) 36143. doi:10.1038/srep36143.

[17] L. Peng, Z. Xu, Z. Liu, Y. Wei, H. Sun, Z. Li, X. Zhao, C. Gao, An iron-based green approach to 1-h production of single-layer graphene oxide, Nat. Commun. 6 (2015) 5716. doi:10.1038/ncomms6716.

[18] D. Marcano, D. Kosynkin, J. Berlin, Improved synthesis of graphene oxide, Acs …. 4 (2010) 4806–14. doi:10.1021/nn1006368.

[19] C.K. Chua, Z. Sofer, M. Pumera, Graphite oxides: Effects of permanganate and chlorate oxidants on the oxygen composition, Chem. - A Eur. J. 18 (2012) 13453–13459. doi:10.1002/chem.201202320.

[20] O. Jankovský, A. Jiříčková, J. Luxa, D. Sedmidubský, M. Pumera, Z. Sofer, Fast Synthesis of Highly Oxidized Graphene Oxide, ChemistrySelect. 2 (2017) 9000–9006. doi:10.1002/slct.201701784.

[21] O. Jankovský, M. Nováček, J. Luxa, D. Sedmidubský, M. Boháčová, M. Pumera, Z. Sofer, Concentration of Nitric Acid Strongly Influences Chemical Composition of Graphite Oxide, Chem. - A Eur. J. 23 (2017) 6432–6440. doi:10.1002/chem.201700809.

[22] A.G. Bannov, A.A. Timofeeva, V. V. Shinkarev, K.D. Dyukova, A. V. Ukhina, E.A. Maksimovskii, S.I. Yusin, Synthesis and studies of properties of graphite oxide and thermally expanded graphite, Prot. Met. Phys. Chem. Surfaces. 50 (2014) 183–190. doi:10.1134/S207020511402004X.

[23] S. Saadat, S. Mansoor, F.I. Kazeminezhad, Effects of initial graphite particle size and shape on oxidation time in graphene oxide prepared by Hummers' method, J. Sci. Adv. Mater. Devices. 2 (2017) 470–475.

[24] M. Inagaki, N. Iwashita, E. Kouno, Potential change with intercalation of sulfuric acid into graphite by chemical oxidation, Carbon N. Y. 28 (1990) 49–55.

[25] G. Beamson, D. Briggs, High resolution XPS of organic polymers, John Wiley & Sons, Chichester, England, 1992.

[26] A. Manakhov, M. Michlíček, A. Felten, J.-J. Pireaux, D. Nečas, L. Zajíčková, XPS depth profiling of derivatized amine and anhydride plasma polymers: Evidence of limitations of the derivatization approach, Appl. Surf. Sci. 394 (2017) 578–585.

doi:10.1016/j.apsusc.2016.10.099.

[27] B. Yuan, L. Song, K.M. Liew, Y. Hu, Mechanism for increased thermal instability and fire risk of graphite oxide containing metal salts, Mater. Lett. 167 (2016) 197–200. doi:10.1016/j.matlet.2015.12.153.

[28] Y. Qui, F. Collin, H.R. Hurt, I. Külaots, Thermochemistry and kinetics of graphite oxide exothermic decomposition for safety in large-scale storage and processing, Carbon N. Y. 96 (2016) 20–28. doi:10.1038/nature13478.

[29] Y. Qiu, S. Moore, R. Hurt, I. Külaots, Influence of external heating rate on the structure and porosity of thermally exfoliated graphite oxide, Carbon N. Y. 111 (2017) 651–657. doi:10.1016/j.carbon.2016.10.051.

[30] F. Kim, J. Luo, R. Cruz-Silva, L.J. Cote, K. Sohn, J. Huang, Self-propagating domino-like reactions in oxidized graphite, Adv. Funct. Mater. 20 (2010) 2867–2873. doi:10.1002/adfm.201000736.

[31] V. Štengl, S. Bakardjieva, J. Henych, L. Kamil, M. Kormunda, Blue and green luminescence of reduced graphene oxide quantum dots, Carbon N. Y. 63 (2013) 537–546. doi:10.1016/j.carbon.2013.07.031.

[32] S. You, S.M. Luzan, T. Szabó, A. V. Talyzin, Effect of synthesis method on solvation and exfoliation of graphite oxide, Carbon N. Y. 52 (2013) 171–180. doi:10.1016/j.carbon.2012.09.018.

[33] M. Mermoux, Y. Chabre, Formation of graphite oxide, Synth. Met. 34 (1989) 157–162.

[34] N. Justh, B. Berke, K. László, I.M. Szilágyi, Thermal analysis of the improved Hummers' synthesis of graphene oxide, J. Therm. Anal. Calorim. (2017). doi:10.1007/s10973-017-6697-2.

[35] S.S. Barton, B.H. Harrison, Acidic surface oxide structures on carbon and graphite-I, Carbon N. Y. 13 (1975) 283–288.

[36] H.-K. Jeong, Y.P. Lee, M.H. Jin, E.S. Kim, J.J. Bae, Y.H. Lee, Thermal stability of graphite oxide, Chem. Phys. Lett. 470 (2009) 255–258. doi:10.1016/j.cplett.2009.01.050.

[37] M. Nováček, O. Jankovský, J. Luxa, D. Sedmidubský, M. Pumera, V. Fila, M. Lhotka, K. Klímová, S. Matějková, Z. Sofer, Tuning of graphene oxide composition by multiple oxidations for carbon dioxide storage and capture of toxic metals, J. Mater. Chem. A. 5 (2017) 2739–2748. doi:10.1039/C6TA03631G.

[38] P.S.V. Jimenez, Thermal decomposition of graphite oxidation products DSC studies of internal combustion of graphite oxide, Mater. Res. Bull. 22 (1987) 601–608.

[39] G.A. Karpenko, V.V. Turov, N.I. Kovtyukhova, É.A. Bakai, A.A. Chuiko, Graphite oxide structure and H2O sorption capacity, Theor. Exp. Chem. 26 (1990) 94–97.

[40] F. Tuinstra, J. Coenig, Characterization of graphite fiber surface with Raman spectroscopy, J

Compos Mater. 4 (1970) 492–499.

[41] A. Ferrari, J. Robertson, Resonant Raman spectroscopy of disordered, amorphous, and diamondlike carbon, Phys. Rev. B. 64 (2001) 1–13. doi:10.1103/PhysRevB.64.075414.

[42] M.S. Dresselhaus, G. Dresselhaus, Intercalation compounds of graphite, Adv. Phys. 30 (1981) 139–326. doi:10.1080/00018738100101367.

[43] H.W. Nesbitt, D. Banerjee, Interpretation of XPS Mn(2p) spectra of Mn oxyhydroxides and constraints on the mechanism of MnO2 precipitation, Am. Mineral. 83 (1998) 305–315. doi:10.2138/am-1998-3-414.

[44] N.E. Sorokina, M.A. Khaskov, V. V. Avdeev, I. V. Nikol'skaya, Reaction of graphite with sulfuric acid in the presence of KMnO4, Russ. J. Gen. Chem. 75 (2005) 162–168. doi:10.1007/s11176-005-0191-4.

[45] N. Sorokina, O. Shornikova, V. Avdeev, Stability limits of graphite intercalation compounds in the systems graphite-HNO3(H2SO4)-H2O-KMnO4, Inorg. Mater. 43 (2007) 822–826. doi:10.1134/S0020168507080031.

[46] J.H. Kang, T. Kim, J. Choi, J. Park, Y.S. Kim, M.S. Chang, H. Jung, K.T. Park, S.J. Yang, C.R. Park, Hidden Second Oxidation Step of Hummers Method, Chem. Mater. 28 (2016) 756–764. doi:10.1021/acs.chemmater.5b03700.

[47] G. Shao, Y. Lu, F. Wu, C. Yang, F. Zeng, Q. Wu, Graphene oxide: The mechanisms of oxidation and exfoliation, J. Mater. Sci. 47 (2012) 4400–4409. doi:10.1007/s10853-012-6294-5.

[48] A.M. Dimiev, J.M. Tour, Mechanism of graphene oxide formation, ACS Nano. 8 (2014) 3060–3068. doi:10.1021/nn500606a.

Tables

Table 1 – Parameters of the sampling during graphite oxide synthesis

Sample	Synthesis time, min	Remarks
GO-1	10	GO-1 sample was collected 10 min after synthesis started before $KMnO_4$ addition
GO-2	30	GO-2 sample was collected after 20 min from $KMnO_4$ addition
GO-3	60	GO-3 sample was collected 30 s before ice addition
GO-4	75	GO-4 sample was collected 30 s before H_2O_2 addition
GO-5	90	GO-5 sample was collected after 15 min from H_2O_2 addition

Table 2 – TGA and DSC data of GO-1 – GO-5 samples heated with a rate of 1 K/min in an argon flow

Sample	Total weight loss, %	GO reduction peak onset, °C	GO reduction peak maximum, °C	GO reduction peak end, °C	Heat release, J/g
GO-1	9.6	-	-	-	-
GO-2	25.08	154	188	214	78
GO-3	33.09	188	210	226	264
GO-4	31.25	184	210	228	198
GO-5	44.0	160	184	202	652

Table 3 – TGA/DSC data of GO-5 samples and their comparison with literature data

Reference	Total weight loss[a], %	DSC peak onset, °C	DSC peak maximum, °C	DSC peak end, °C	Heat release[b], J/g	Method of synthesis	Gas atmosphere of TGA/DSC measurements (flow rate)
This article	44	160	184	202	652	Modified Hummers' method	Ar (200 cm^3/min)
[3]	28	n/a	558	n/a	1080	Brodie method	N_2 (n/a)
[28]	n/a	150	n/a	n/a	1600	Modified Hummers' method	N_2 (n/a)
[29]	n/a	n/a	~180	n/a	1360	Modified Hummers' method	n/a
[30]	n/a	n/a	~210	n/a	6000–8000	Modified Hummers' method	N_2 (n/a)
[31]	58	142	182	300	n/a	Modified Hummers' method	air (75 cm^3/min)
[32]	56.7	195	213	n/a	1200–1300	Hummers' method	N_2 (n/a)
[32]	41.8	~240	281	n/a	1200–1300	Brodie method	N_2 (n/a)

[a] – The value was determined by TGA;

[b] – The value depends on the heating rate.

Table 4 – Raman spectroscopy data

Sample	D peak position, cm^{-1}	D_{FWHM}, cm^{-1}	G peak position, cm^{-1}	G_{FWHM}, cm^{-1}	I(D)/I(G)
GO-1	1349.4±0.2	130.85±0.7	1576.2±0.1	22.24±0.3	0.092
GO-2	n/a	n/a	1570±1.1	36±2.3	n/a[a]
GO-3	1358.5±0.4	174±1.2	1580.8±0.2	80.7±0.7	0.91
GO-4	1358.2±0.4	161.5±1.1	1587.2±0.2	73.1±0.7	0.87
GO-5	1356.1±0.4	120.2±1.3	1590.5±0.3	70.3±0.9	0.88

[a] – It was not possible to estimate the parameters of GO-2 Raman spectrum due to strong luminescence.

Table 5 – Results of the fitting of the C1s XPS spectra of the samples and the elemental composition of the samples

Sample	Components of C1s peak, at.%						Concentration of elements, at.%				O:C (at.)
	C=C (sp^2)	C–H	C–O	C=O	COOH	Shake-up	C	O	S	Mn	
GO-1	87.5±3.5	-	-	6.0±1.8	3.3±1.6	3.2±1.4	93.3±3.5	6.2±0.2	0.5±0.2	0.0	0.06
GO-2	53.8±7.9	11.6±7.0	16.2±3.3	6.7±2.2	11.8±4.2	-	26.9±1.0	51.6±1.8	0.5±0.2	18.7±0.8	1.92
GO-3	31.2±2.9	15.3±3.2	29.7±3.4	15.8±4.3	8.1±3.3	-	46.1±1.2	44.2±0.9	0.0	9.7±0.9	0.96
GO-4	20.3±1.0	14.3±0.8	29.9±0.9	14.3±1.3	14.7±1.3	6.5±1.0	69.5±1.9	29.8±0.7	0.7±0.1	0.0	0.43
GO-5	13.9±0.9	17.3±1.2	33.6±1.0	15.7±0.9	15.9±1.2	3.7±1.3	67.6±0.7	31.9±0.4	0.6±0.1	0.0	0.47